Vacuum 217 (2023) 112554

Contents lists available at ScienceDirect

Vacuum

journal homepage: www.elsevier.com/locate/vacuum

Developing a practice for the heat treatment of laser-powder bed fused Ti-6Al-2Sn-4Zr-2Mo-0.08Si alloy

Harish Chandra Kaushik [a], Mahdi Habibnejad Korayem [b], Amir Hadadzadeh [a,*]

[a] Department of Mechanical Engineering, University of Memphis, Memphis, TN, USA
[b] AP&C Advanced Powder and Coating, a GE Additive Company, Montreal, Quebec, Canada

ARTICLE INFO

Handling Editor: Mr. Paul Mayrhofer

Keywords:
Laser-powder bed fusion
Titanium alloys
Heat treatment
Strength
Ductility

ABSTRACT

The laser-powder bed fusion (L-PBF) technique is employed to print cylindrical rods of near-α Ti-6Al-2Sn-4Zr-2Mo-0.08Si (Ti6242) alloy. The parts are printed using four scan speeds; 1000, 1200, 1400, and 1600 mm/s. Since the 1200 mm/s sample possesses the highest strength in the as-built condition, it is selected as the benchmark sample for heat treatment development. The kinetics of α to β phase transformation is employed in designing a two-step sub-transus heat treatment recipe. The mechanical properties and microstructure of both as-built and heat-treated parts are studied to elaborate on the process-microstructure-properties relationship and the effectiveness of the heat treatment recipe. In the next step, this recipe is applied to the other samples. The formulated heat treatment works effectively for all conditions and makes the final properties more uniform. This study shows the effectiveness of developing a heat treatment for one printing condition and extending it to other printing conditions.

1. Introduction

Titanium and its alloys have applications in a wide range of industries including aerospace, defense, transportation, biomedical, etc. [1]. Ti-6Al-4V (Ti64) is the most common α+β titanium alloy [2] with a good strength-ductility synergy at room and elevated temperatures up to 400 °C [3]. For temperatures above 400 °C, Ti64 exhibits a significant strength loss which limits its application. Therefore, high-strength near-α titanium alloys are considered for these conditions [4]. Ti-6Al-2Sn-4Zr-2Mo-0.08Si (Ti6242) is a near-α titanium alloy that retains its strength at high temperatures up to 540 °C [5]. The fabrication of Ti6242 components through conventional manufacturing processes has a long history [6]; however, few studies are available on the laser-powder bed fusion (L-PBF) of this alloy [5,7–13]. The ultrahigh cooling rates associated with the L-PBF process, in the range of 10^3–10^8 K/s [14], result in the evolution of an ultrafine α' martensitic structure, featured by pre-existing dislocation networks and nanotwins [5,9,13]. These ultrafine microstructural characteristics significantly enhance the strength of the L-PBF-Ti6242 parts; however, the resulting ductility is very low [8,12]. Therefore, post-process heat treatment recipes have been developed to enhance the ductility of the L-PBF-Ti6242 [9,10,12].

The common practice in developing the heat treatments for L-PBF-Ti6242 is to print the sample using one set of process parameters, heat treat the sample, and characterize the resulting mechanical properties and microstructure. This is also a common practice for other alloying systems including Ti64 [15], aluminum alloys [16], and steels [17]. It is well-established that the microstructure of L-PBF alloys is dependent on the process parameters [18]. Changing the process parameters will alter the thermal boundaries and cooling conditions which then alter the resulting microstructure [19]. Therefore, both physical and mechanical properties will change. As a result, a concern is raised; if a heat treatment is developed for a set of L-PBF process parameters, is it effectively applicable to samples printed by other process parameters?

In the current study, we aim to address the above-mentioned question. To do so, cylindrical rods of Ti6242 are printed using four sets of L-PBF process parameters. One sample is selected as the benchmark and a two-step heat treatment recipe is developed considering the kinetics of phase transformation in the sample. The microstructure and mechanical properties of the heat-treated benchmark sample are studied to elaborate on the strengthening and toughening mechanism. The formulated heat treatment recipe is then applied to the other samples to investigate its applicability.

* Corresponding author.
E-mail address: amir.hadadzadeh@memphis.edu (A. Hadadzadeh).

https://doi.org/10.1016/j.vacuum.2023.112554
Received 9 May 2023; Received in revised form 14 July 2023; Accepted 26 August 2023
Available online 29 August 2023

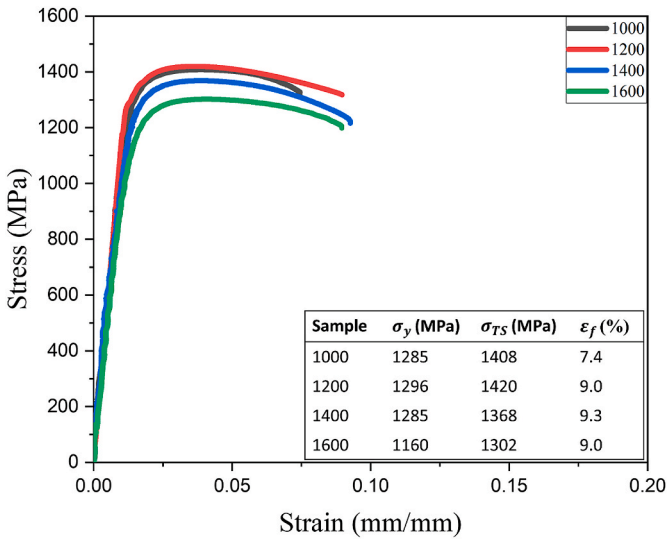

Fig. 1. Tensile properties of AB-L-PBF-Ti6242.

2. Materials and methods

Cylindrical rods of Ti6242 with the nominal composition of Ti-6Al-2Sn-4Zr-2Mo-0.08Si (wt.%) were printed using an EOS-M290 system. The rods were printed vertically with dimensions of 8 mm (diameter) × 70 mm (height). Since EOS has not developed the process parameters for the Ti6242 system, the available parameters for Ti64 were employed [20]. The main L-PBF process parameters that determine the energy density include laser power (P in W), scan speed (v in mm/s), hatch distance (l in μm), and layer thickness (h in μm). These parameters were set to $P = 280$ W, $l = 140$ μm, and $h = 30$ μm. To vary the energy density, the samples were printed using four scan speeds; $v = 1000$, 1200, 1400, and 1600 mm/s. The samples are designated as 1000, 1200, 1400, and 1600, respectively. All samples were printed under Ar protective atmosphere, using the stripe scanning strategy.

The relative density of the samples was measured using the Archimedes method following ASTM B311-22 standard [21]. The relative density of 1000, 1200, 1400, and 1600 samples was determined as 99.4%, 99.6%, 99.3%, and 99.3%, respectively. As seen all samples were printed with the least defects.

The cylindrical rods were heat treated in a Lindberg Blue M furnace by Thermo Scientific. Tensile testings were carried out following the ASTM E8/E8M-21. Dogbone samples with a gauge length of 16 mm and a diameter of 4 mm were pulled using a Shimadzu Autograph AGS-X (Shimadzu, Kyoto, Japan) universal testing system, with a constant strain rate of 0.5%/min. The tensile samples were machined from the rods, therefore, the effect of surface roughness was not taken into account. Each tensile test for the as-built samples was repeated three times. The mean values and standard deviation analysis showed that the error is less than 1.2% for strength and 5% for ductility. Due to the consistency of the results, the rest of the tensile tests (for the heat-treated samples) were not repeated, unless any inconsistencies or outliers were observed.

The hardness of the samples was measured using the Rockwell C hardness (HRC) technique by applying a 150 kgf load using a Wilson instrument (an Instron Company). The measurements were repeated five times for each sample and the average value is reported.

The microstructure was studied using the transmission electron microscopy (TEM) technique by employing a Thermo Scientific Talos 200X equipped with an X-FEG source and an adjustable high tension between 80 and 200 kV. The sample preparation was completed through ion milling and the TEM images were taken along the building direction. Both TEM and scanning TEM (STEM) modes were used for imaging. All images were taken in the bright-field (BF) mode.

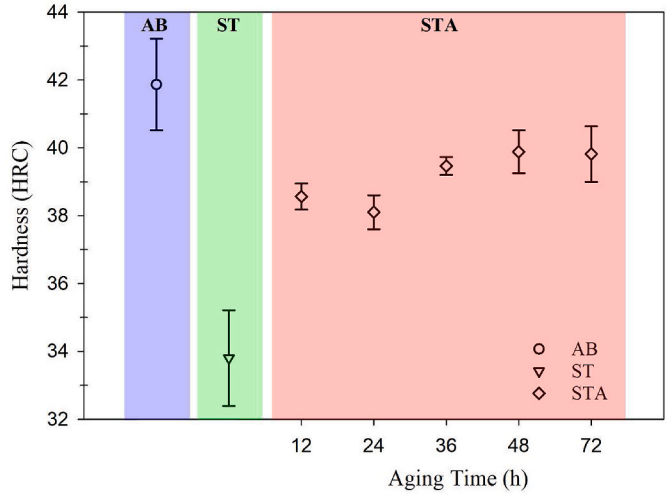

Fig. 2. The hardness of sample 1200 in the AB, ST, and STA conditions.

3. Results and discussion

The tensile properties of as-built (AB) L-PBF-Ti6242 are shown in Fig. 1. Some variations in strength and ductility are observed, which stem from applying different energy densities in printing the parts. The yield strength (σ_y), tensile strength (σ_{TS}), and strain at fracture (ε_f) of the AB rods are summarized in the inset. Samples 1200 and 1600 possess the highest and lowest strengths, respectively. The difference between the lowest and highest σ_y and σ_{TS} are 136 MPa and 118 MPa, respectively. The level of ε_f is almost the same for 1200, 1400, and 1600 samples. Sample 1000 possesses the lowest ε_f, which brings the difference between the highest and lowest ε_f to 1.9%. Considering the relative density of the AB samples (99.3–99.6%), it appears that the defects may not dominate the ductility of the material. Rather, the microstructure governs the quasi-static mechanical properties, including both strength and ductility. In fact, different strengthening/toughening mechanisms are active in different length scales due to the complex and hierarchical microstructure developed during the rapid solidification [19]. To elaborate on the role of each microstructural feature (and/or defects) on the ductility of the material, more in-depth analysis is required. Considering the synergy of strength and ductility, sample 1200 appears to be printed using the optimum conditions (among those selected for the current study). Therefore, this sample was selected to investigate the kinetics of α to β phase transformation in our previous study [22].

The basis for the design of heat treatment recipes for Ti6242 is the controlled nucleation and growth of the β phase to achieve synergistic strength and ductility [10]. In the current study, another factor was taken into account; preserving the hierarchical and ultrafine characteristics of the microstructure, with an emphasis on the nanotwins and dislocations. Therefore, long exposure to high temperatures should be avoided. Instead, a two-step sub-transus heat treatment was designed which comprised a short exposure to a high temperature close to the β-transus, followed by a long exposure to a moderate temperature below the annihilation temperature of the nanotwins. The annihilation of nanotwins occurs at ~500–600 °C [22]. The first step results in the nucleation and the second step results in the growth of the β phase. Therefore, to formulate the heat treatment recipe for the L-PBF-Ti6242, the isothermal α to β phase transformation kinetics was considered as follows [23],

$$f = 1 - \exp\left[-(kt)^n\right] \quad (1)$$

where f is the fraction of the transformed β at a given time (t) after the transformation starts, n is the Avrami exponent, and k is the temperature-dependent rate constant which is determined as follows

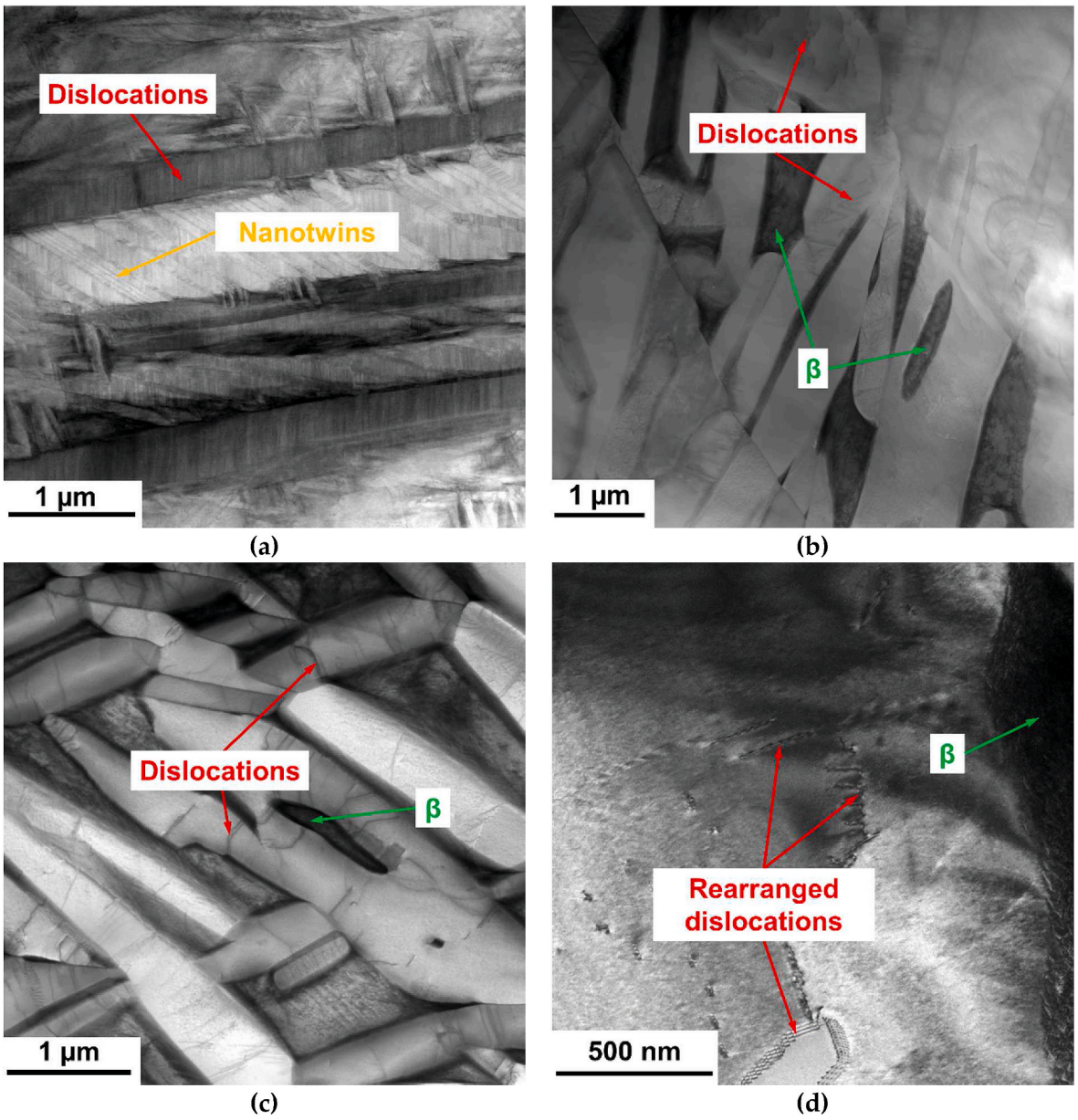

Fig. 3. STEM-BF micrograph of sample 1200 in the (a) AB, (b) ST, and (c) STA conditions, (d) TEM-BF micrograph of STA sample showing the details of rearranged dislocations.

[24],

$$k(T) = k_0 \, exp\left(-\frac{E_a}{RT}\right) \tag{2}$$

where E_a is the activation energy for transformation, T is temperature, R is the universal gas constant, and k_0 is the pre-exponential factor. For the 1200 sample, the parameters in Eqs. (1) and (2) were determined as $n = 0.75$, $k_0 = 2.55 \times 10^{38}$, and $E_a = 973.73$ kJ/mol [22]. By employing the kinetics model, it was determined that if the sample is held at 900 °C for 10 min, about 2% β will form. Therefore, the first step of the heat treatment was holding at 900 °C for 10 min followed by water quenching. This step is designated as the sub-transus (ST) stage. In the next step, the sample was aged at 300 °C for 12–72 hours, since at 300 °C both dislocations and nanotwins are preserved. The sample after the aging treatment is designated as ST aged (STA). The hardness values of AB, ST, and STA samples were measured and reported in Fig. 2. The highest hardness belongs to the AB-L-PBF-Ti-6242. ST treatment substantially reduced the hardness. Following the aging step, the hardness was enhanced; however, some fluctuations are observed in the hardness values. By comparing the hardness of the aged samples, 48 hours of holding was identified as the desired aging time since it resulted in the maximum hardness.

The mechanical properties of the ST sample were $\sigma_y = 883$ MPa, $\sigma_{TS} = 1102$ MPa, and $\varepsilon_f = 17.5\%$. 10 min of holding at 900 °C significantly improved the ductility at the expense of strength. On the other hand, the aging treatment changed the properties of the STA sample to $\sigma_y = 1055$ MPa, $\sigma_{TS} = 1147$ MPa, and $\varepsilon_f = 14.7\%$. As seen, the aging treatment increased the strength with some extent of ductility loss.

The microstructures of AB, ST, and STA samples were studied in the scanning mode of TEM (STEM) and the bright field (BF) images are shown in Fig. 3. As seen, the microstructure of AB-L-PBF-Ti6242 consists of fine α′ martensite lath with a width of less than 1 μm. The pre-existing dislocation networks and nanotwins developed within the martensite lath as a result of rapid solidification [5,25]. Fine α' laths with a distorted crystal structure and dense dislocations (*i.e.,* networks of tangled dislocations with high density) are the main strengthening mechanisms

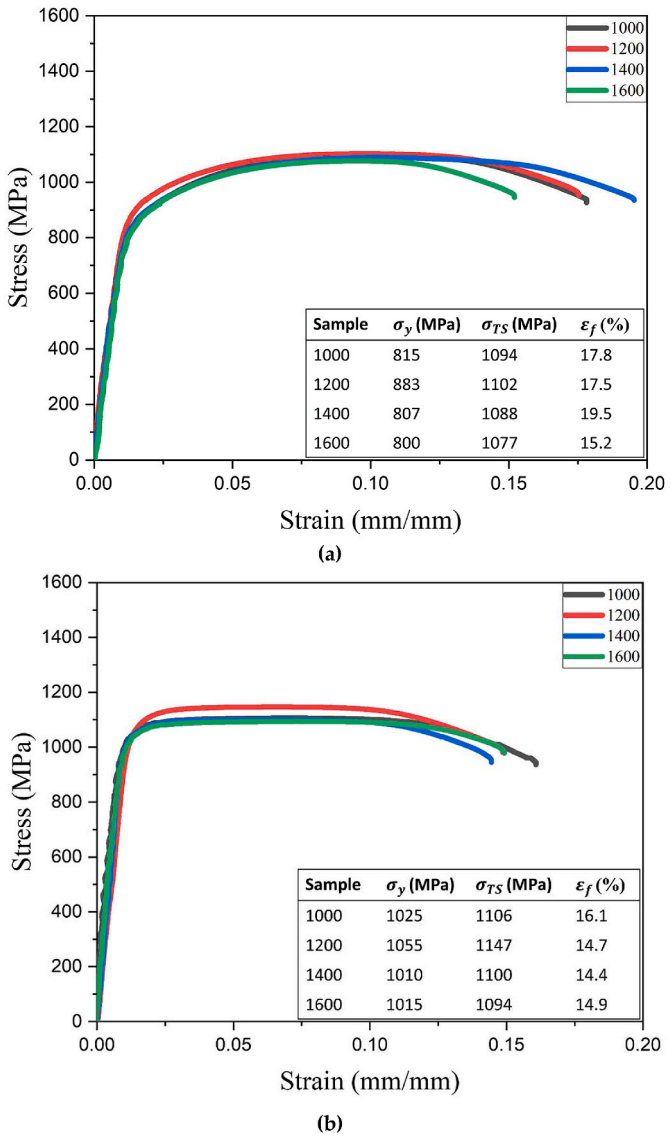

Fig. 4. Tensile properties of (a) ST and (b) STA samples.

in the AB sample [7]. Nanotwins mainly contribute to ductility as they increase the dislocation storage capacity of the material [26]. The short hold at 900 °C resulted in the nucleation of the β phase with a bcc crystal structure [12]. The evolution of the β phase in the ST sample contributes to ductility improvement [12]. The dislocations within the martensite laths are still observed in the ST sample, due to the short holding time.

After the aging step, the dislocations rearranged their configuration in the martensite lath and developed dislocation arrays, as observed in Fig. 3 (c). The details of rearranged dislocations were studied in the TEM mode, as shown in Fig. 3 (d). These arrays act as barriers against dislocation motion and enhance the strength of the STA sample. The governing mechanism is the reduction of the mean effective slip length of the dislocations. In other words, a Hall-Petch-like mechanism is activating in the STA-L-PBF-Ti-6242 by developing the dislocation arrays [27].

The heat treatment recipe was formulated by employing the kinetics model developed specifically for the sample printed with $v = 1200$ mm/s. By changing the scan speed, the cooling conditions will change which then alters the microstructure. Therefore, the physical properties and consequently the kinetics of α to β phase transformation will be different in 1000, 1400, and 1600 samples. To assess the applicability of the formulated heat treatment recipe to the other samples, 1000, 1400, and 1600 rods were heat treated using the same recipe, and the tensile properties are shown in Fig. 4. The key mechanical properties of the heat-treated samples are summarized in the insets.

As seen in the stress-strain curves of the samples, the ST heat treatment enhanced the ductility of all samples accompanied by strength loss. The level of ductility improvement was not the same in all samples. Moreover, the level of strength reduction was not consistent in all samples. The difference between the lowest and highest σ_y, σ_{TS}, and ε_f in the ST samples are 83 MPa, 25 MPa, and 4.3%, respectively. The aging step increased the yield strength of all samples between 172 MPa and 215 MPa. A slight increase in the tensile strength and a slight reduction in the ductility is observed. The difference between the lowest and highest σ_y, σ_{TS}, and ε_f in the STA samples are 45 MPa, 53 MPa, and 1.7%, respectively. Therefore, the STA heat treatment not only worked effectively for all conditions but also made the final properties more uniform (compared to the as-built condition).

4. Conclusions

The near-α Ti6242 alloy was printed using the L-PBF process with four different energy densities by varying the scan speed between 1000 and 1600 mm/s. The mechanical properties of the as-built samples showed that a scan speed of 1200 mm/s resulted in the highest strength (*i.e.*, σ_y =1296 MPa and σ_{TS} = 1420 MPa). Therefore, this sample was selected as the benchmark for the design of a heat treatment recipe. The kinetics of α to β phase transformation in this sample was employed to formulate a two-step sub-transus heat treatment consisting of a sub-transus (ST) holding at 900 °C for 10 min followed by aging at 300 °C for 48 hours (STA). The STA heat treatment effectively enhanced the ductility of the sample from 9% to 14.7%. The yield and tensile strengths of the STA sample were also 1055 MPa and 1147 MPa, respectively. To assess the applicability of the designed heat treatment to the other printing conditions, 1000, 1400, and 1600 samples were heat treated using the same recipe. The STA heat treatment effectively and consistently improved the ductility of all samples and meanwhile made the strengths of all samples more uniform. While the difference between the lowest and highest σ_y and σ_{TS} in the as-built samples were 136 MPa and 118 MPa, respectively, the associated differences were 45 MPa and 53 MPa in the STA samples. Therefore, this study shows that if a heat treatment recipe is developed for one printing condition, it can be applied effectively to the other printing conditions.

CRediT authorship contribution statement

Harish Chandra Kaushik: Writing – review & editing, Methodology, Investigation, Formal analysis. **Mahdi Habibnejad Korayem:** Writing – review & editing, Resources, Conceptualization. **Amir Hadadzadeh:** Writing – original draft, Supervision, Methodology, Investigation, Funding acquisition, Formal analysis, Conceptualization.

Declaration of competing interest

The authors declare that they have no known competing financial interests or personal relationships that could have appeared to influence the work reported in this paper.

Data availability

The data that has been used is confidential.

Acknowledgment

The authors would like to acknowledge the Herff College of Engineering at the University of Memphis for the financial support of a part of the research through the HCOE-FRG program. The authors would like

to acknowledge Dr. Fotovvati and Dr. Asadi at the Metal Additive Manufacturing Laboratory at the University of Memphis for facilitating the fabrication of the L-PBF components.

References

[1] C. Veiga, J.P. Davim, A.J.R. Loureiro, Properties and applications of titanium alloys: a brief review, Rev. Adv. Mater. Sci. 32 (2012) 14–34.

[2] S. Liu, Y.C. Shin, Additive manufacturing of Ti6Al4V alloy: a review, Mater. Des. 164 (2019), 107552, https://doi.org/10.1016/j.matdes.2018.107552.

[3] H. Chandler, Heat Treater's Guide: Practices and Procedures for Ferrous Alloys, ASM International, 1996.

[4] P.J. Postans, F.H. Froes, High temperature titanium alloys-A review, JOM 36 (1984) 55–62, https://doi.org/10.1007/BF03338617.

[5] C. Fleißner-Rieger, T. Pfeifer, T. Jörg, T. Kremmer, M. Brabetz, H. Clemens, S. Mayer, Selective laser melting of a near-α Ti6242S alloy for high-performance automotive parts, Adv. Eng. Mater. 23 (2021), 2001194, https://doi.org/10.1002/adem.202001194.

[6] E.L. Odenberger, R. Pederson, M. Oldenburg, Thermo-mechanical material response and hot sheet metal forming of Ti-6242, Mater. Sci. Eng. A 489 (2008) 158–168, https://doi.org/10.1016/j.msea.2007.12.047.

[7] H. Fan, S. Yang, Effects of direct aging on near-alpha Ti–6Al–2Sn–4Zr–2Mo (Ti-6242) titanium alloy fabricated by selective laser melting (SLM), Mater. Sci. Eng. A. 788 (2020), 139533, https://doi.org/10.1016/j.msea.2020.139533.

[8] H. Fan, Y. Liu, S. Yang, Martensite decomposition during post-heat treatments and the aging response of near-α Ti–6Al–2Sn–4Zr–2Mo (Ti-6242) titanium alloy processed by selective laser melting (SLM), J. Micromechanics Mol. Phys. 6 (2021), 2050018, https://doi.org/10.1142/S2424913020500186.

[9] Z. Zhu, F.L. Ng, H.L. Seet, S.M.L. Nai, Tailoring the microstructure and mechanical property of laser powder bed fusion fabricated Ti–6Al–2Sn–4Zr–2Mo via heat treatment, J. Alloy. Compd. 895 (2022), 162648, https://doi.org/10.1016/j.jallcom.2021.162648.

[10] C. Fleißner-Rieger, T. Pfeifer, C. Turk, H. Clemens, Optimization of the post-process heat treatment strategy for a near-α titanium base alloy produced by laser powder bed fusion, Materials 15 (2022) 1032, https://doi.org/10.3390/ma15031032.

[11] C. Fleißner-Rieger, M.A. Tunes, C. Gammer, T. Jörg, T. Pfeifer, M. Musi, F. Mendez-Martin, H. Clemens, On the existence of orthorhombic martensite in a near-α titanium base alloy used for additive manufacturing, J. Alloy. Compd. 897 (2022), 163155, https://doi.org/10.1016/j.jallcom.2021.163155.

[12] Z. Zhu, P. Kumar, F.L. Ng, H.L. Seet, U. Ramamurty, S.M.L. Nai, Heat treatment effect on the microstructure and elevated temperature tensile property of the Ti6242S alloy fabricated via laser powder bed fusion, J. Alloy. Compd. 925 (2022), 166656, https://doi.org/10.1016/j.jallcom.2022.166656.

[13] C. Fleißner-Rieger, H. Schönmaier, M. Musi, M. Stadler, H. Gschiel, C. Turk, T. Pfeifer, H. Clemens, Formation and evolution of precipitates in an additively manufactured near-α titanium base alloy, Materialia 21 (2022), 101366, https://doi.org/10.1016/j.mtla.2022.101366.

[14] D. Herzog, V. Seyda, E. Wycisk, C. Emmelmann, Additive manufacturing of metals, Acta Mater. 117 (2016) 371–392, https://doi.org/10.1016/j.actamat.2016.07.019.

[15] C. de Formanoir, G. Martin, F. Prima, S.Y.P. Allain, T. Dessolier, F. Sun, S. Vives, B. Hary, Y. Brechet, S. Godet, Micromechanical behavior and thermal stability of a dual-phase α+α' titanium alloy produced by additive manufacturing, Acta Mater. 162 (2019) 149–162, https://doi.org/10.1016/j.actamat.2018.09.050.

[16] J. Fite, S.E. Prameela, J.A. Slotwinski, T.P. Weihs, Evolution of the microstructure and mechanical properties of additively manufactured AlSi10Mg during room temperature holds and low temperature aging, Addit. Manuf. 36 (2020), 101429, https://doi.org/10.1016/j.addma.2020.101429.

[17] J. Zhang, M. Wang, L. Niu, J. Liu, J. Wang, Y. Liu, Z. Shi, Effect of process parameters and heat treatment on the properties of stainless steel CX fabricated by selective laser melting, J. Alloy. Compd. 877 (2021), 160062, https://doi.org/10.1016/j.jallcom.2021.160062.

[18] H. Rao, S. Giet, K. Yang, X. Wu, C.H.J. Davies, The influence of processing parameters on aluminium alloy A357 manufactured by Selective Laser Melting, Mater. Des. 109 (2016) 334–346, https://doi.org/10.1016/j.matdes.2016.07.009.

[19] T. DebRoy, H.L. Wei, J.S. Zuback, T. Mukherjee, J.W. Elmer, J.O. Milewski, A. M. Beese, A. Wilson-Heid, A. De, W. Zhang, Additive manufacturing of metallic components – process, structure and properties, Prog. Mater. Sci. 92 (2018) 112–224, https://doi.org/10.1016/j.pmatsci.2017.10.001.

[20] B. Fotovvati, S.A. Etesami, E. Asadi, Process-property-geometry correlations for additively-manufactured Ti–6Al–4V sheets, Mater. Sci. Eng. A 760 (2019) 431–447, https://doi.org/10.1016/j.msea.2019.06.020.

[21] ASTM B311-17, Standard Test Method for Density of Powder Metallurgy (PM) Materials Containing Less than Two Percent Porosity, ASTM International, West Conshohocken, PA, USA, 2017. Available online: www.astm.org.

[22] H.C. Kaushik, M. Habibnejad Korayem, A. Hadadzadeh, Determination of α to β phase transformation kinetics in laser-powder bed fused Ti–6Al–2Sn–4Zr–2Mo-0.08Si and Ti–6Al–4V alloys, Mater. Sci. Eng., A 860 (2022), 144294, https://doi.org/10.1016/j.msea.2022.144294.

[23] J. Farjas, P. Roura, Modification of the Kolmogorov-Johnson-Mehl-Avrami rate equation for non-isothermal experiments and its analytical solution, Acta Mater. 54 (2006) 5573–5579, https://doi.org/10.1016/j.actamat.2006.07.037.

[24] H. Li, K. Gai, L. He, C. Zhang, H. Cui, M. Li, Non-isothermal phase-transformation kinetics model for evaluating the austenization of 55CrMo steel based on Johnson-Mehl-Avrami equation, Mater. Des. 92 (2016) 731–741, https://doi.org/10.1016/j.matdes.2015.12.110.

[25] H. Eskandari Sabzi, X.H. Li, C. Zhang, H. Fu, D. San-Martin, E. Pedro, J. Rivera-Diaz-del-Castillo, Deformation twinning-induced dynamic recrystallization during laser powder bed fusion, Scripta Mater. 207 (2022), 114307, https://doi.org/10.1016/j.scriptamat.2021.114307.

[26] K. Lu, L. Lu, S. Suresh, Strengthening materials by engineering coherent internal boundaries at the nanoscale, Science 324 (5925) (2009) 349–352, https://doi.org/10.1126/science.1159610.

[27] W. Zhu, J. Lei, C. Tan, Q. Sun, W. Chen, L. Xiao, J. Sun, A novel high-strength β-Ti alloy with hierarchical distribution of α-phase: the superior combination of strength and ductility, Mater. Des. 168 (2019), 107640, https://doi.org/10.1016/j.matdes.2019.107640.